International Journal of Advanced Engineering and Management Research
Vol. 3 Issue 5; 2018

www.ijaemr.com ISSN: 2456-3676

PREDICTION AND OPTIMIZATION OF WELD MOLTEN METAL FLUIDITY OF TIG MILD STEEL WELD USING RESPONSE SURFACE METHODOLOGY

Anowa, H.D,Achebo, J.IObahiagbon K.O. And Osarenmwinda J.O.
Department of Production Engineering, University of Benin, Benin City, Nigeria

(Anowa, H.D), (Achebo, J.I) (Obahiagbon K.O), (Osarenmwinda)

Abstract

Structures produced as a result of poor weld molten metal fluidity do not possess enough strength required to sustain its useful service life. This study was carried out with the aim of optimizing and predicting the weld molten metal fluidity of weldment. Mild steel plate was cut into dimension 60mmx40mmx10mm with a power hacksaw, grinded and cleaned before the welding process. The experimental matrix was made of twenty (20) runs, generated by the design expert 7.01 software adopting the central composite design. The responses were measured; molten metal fluidity then modelled using the response surface methodology. The result obtained in this research study shows that high molten metal fluidity produce weldment with better structural integrity. The model produced numerical optimal solution of current 150 amps, voltage of 20 volts and gas flow rate of 17l/min will produce a welded structure having molten metal fluidity of 143.33ms/kg at a desirability value of 94.6%.

Keyword: Fluidity, weld, molten metal and RSM

Introduction

Flow ability of weld molten metal from its liquid state to solid state during solidification is somewhat similar to the metal casting solidification process Bakir et al. (2018) and Choo (1992).Moran do et al.(2015) and Di Sabatino et al.(2008) defines fluidity of molten met alas the distance a molten metal can cover before solidifying. Tailoring it into welding, we can define fluidity of a weld as the distance a molten metal can travel into the gap between the mating surfaces of parent metals during welding before solidification. This molten metal possess a constant cross sectional area before it solidifies Kou and Wang (1986).Moran do et al.(2015) noted that in filling thin sections with molten metal, flow ability is limited by heat transfer. Molten metal fluidity can as well be used to describe the depth of penetration of molten metal, Kou et al. (2011) and Chen and Kovacevic (2004). Molten metal fluidity consists of two basic factors which includes the characteristic molten metal and the welding process parameters. Also fluidity is inversely proportional to weld pool's solidification range, Bakhtiyarov and Over felt(1999) and Ambroziak (1999). Di Sabatino et al. (2008) wrote that fluidity limits the cast ability of alloys and the final properties of castings, fluidity problems in welding results in poor surface finish and wall thickness problems. Poor or insufficient fluidity affects the soundness of cast products or welded joints and is detrimental to the final quality of the cast component or weldments. There is therefore, a strong industrial demand for understanding the physical and process parameters governing the fluid flow of casting or weld alloys in order to improve their fluidity. Davies (1992) said that it is difficult to experimentally determine the flow within a weld pool because of the unfriendly local environment (arc thermal cycle), and the material concerned. Liquid metal is not transparent so at best only surface flow can be observed. This prevents a simple study of the crucial recirculating regions within the pool and the flow conditions at the solid-liquid interface. Hence there is a great practical need for numerical flow models in order to further improve our understanding of weld pool behavior. With the significant advances in computer hardware and software over recent years such models once programmed as computer simulations can now provide a previously unobtainable insight into weld pool flow Chen and Kovacevic (2004).

The characteristics of molten metal which influences fluidity include the viscosity, surface tension, and the solidification pattern of the alloy. As viscosity and its sensitivity to temperature (viscosity index) increase, fluidity decreases. A high surface tension of the liquid metal reduces fluidity. That is, oxide films developed on the surface of the molten metal known as slag have a significant effect on fluidity. For instance, the slag on the surface of pure molten aluminum triples its surface tension. . Thus the shorter the range (as in pure metals and eutectics), the higher the fluidity becomes. Conversely, alloys with long solidification ranges (such as solid solution alloys) have lower fluidity. Optimizing these parameters would further drastically reduce or eliminate some of the problems associated with poor fluidity and also promotes scrap reduction, or reduction of weld undercuts, which in turn leads to greater efficiency and increased profitability.

Materials and Methods

Materials

100 pieces of mild steel coupons measuring 80 x 40 x10 was used for the experiments, the experiment was performed 20 times using 5 specimens for each run. The key parameters considered in this work are welding current, welding speed, gas flow rate, and welding voltage. The range of the process parameters obtained from literature which is shown in the table 1. The tungsten inert gas welding equipment was used to weld the plates after the edges have been bevelled and machined. Figure 1 shows the TIG welding setup. The welding process uses a shielding gas to protect the weld specimen from atmospheric interaction, 100% pure Argon gas was used in this research study. Figure 2 shows the shielding gas cylinder and regulator. Figure 3 shows the weld sample

Figure 1: TIG equipment

Figure 2: shielding gas cylinder and regulator

Table 1: Process parameters and their levels

Factors	Unit	Symbol	Low (-1)	High (+1)
Welding Current	Ampere	I	130	170
Welding Voltage	Volts	V	20	24
Gas Flow Rate	Lit/min	GFR	13	17

Figure 3 weld samples

Method of Data Collection

The central composite design matrix was developed using the design expert software, producing 20 experimental runs. The input parameters and output parameters make up the experimental matrix and the responses recorded from the weld samples was used as the data. The data matrix is determined by the number of input parameters which is expressed in the equation 2n +2n +k, where k is number of center points,2n is the number of axial points and 2nis the number of factorial points.

The matrix expressed in actual values which fall within the range stated, is presented in figure 4

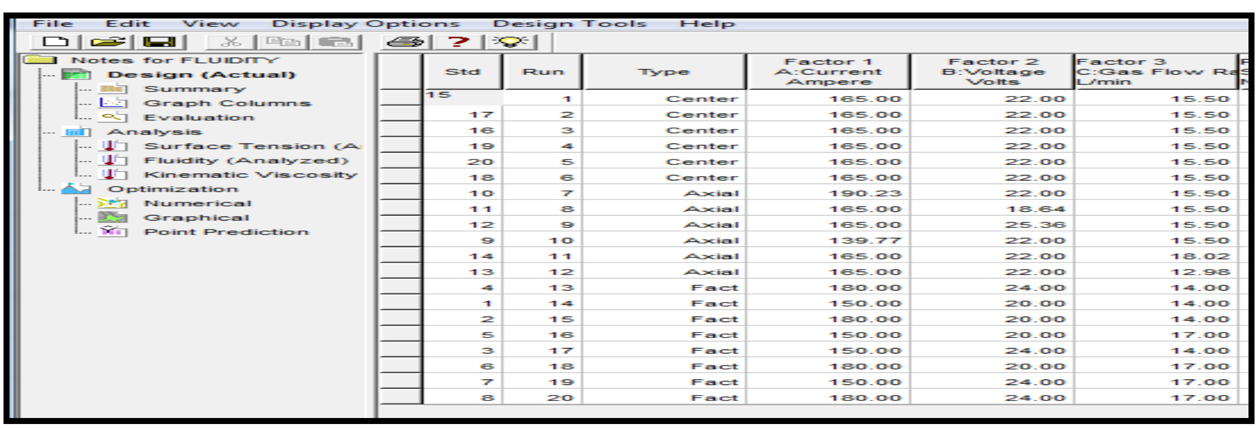

Std	Run	Type	Factor 1 A:Current Ampere	Factor 2 B:Voltage Volts	Factor 3 C:Gas Flow Ra L/min
15	1	Center	165.00	22.00	15.50
17	2	Center	165.00	22.00	15.50
16	3	Center	165.00	22.00	15.50
19	4	Center	165.00	22.00	15.50
20	5	Center	165.00	22.00	15.50
18	6	Center	165.00	22.00	15.50
10	7	Axial	190.23	22.00	15.50
11	8	Axial	165.00	18.64	15.50
12	9	Axial	165.00	25.36	15.50
9	10	Axial	139.77	22.00	15.50
14	11	Axial	165.00	22.00	18.02
13	12	Axial	165.00	22.00	12.98
4	13	Fact	180.00	24.00	14.00
1	14	Fact	150.00	20.00	14.00
2	15	Fact	180.00	20.00	14.00
5	16	Fact	150.00	20.00	17.00
3	17	Fact	150.00	24.00	14.00
6	18	Fact	180.00	20.00	17.00
7	19	Fact	150.00	24.00	17.00
8	20	Fact	180.00	24.00	17.00

Figure 4 Central Composite Design Matrix (CCD) in actual values

Testing the adequacy of the models developed

Table 2 shows the analysis of variance component, the analysis of variance (ANOVA) was used to test the adequacy of the models. The statistical significance of the models developed and each term in the regression equation were examined using the sequential F-test, lack-of-fit test and other adequacy measures (i.e. R2, Adj- R~, Pred. R2 and Adeq. Precision ratio) using the same software to obtain the best fit. The Prob.>F (sometimes called p-value) of the model and of each term in the model can be computed by means of ANOVA.

Table 2: Analysis of Variance Components

Variation Source	**Degree of Freedom Df**	**Sum of Squares SS**	**Mean Square MS**	**Fisher Ratio F-value**
Error of residuals	n-2	$SSE = \sum_{i=1}^{c}\sum_{j=1}^{ni}(y_{ij} - \hat{y}_{ij})^2$	$MSE = \frac{SSE}{n-2}$	
Regression	1	$SSR = \sum_{i=1}^{c}\sum_{j=1}^{ni}(\hat{y}_{ij} - \bar{y})^2$	$MSR = \frac{SSR}{1}$	$F = \frac{MSR}{MSE}$
Lack of fit	C -2	$SSLF_i = \sum_{i=1}^{c}\sum_{j=1}^{ni}(\bar{y}_{ij} - \hat{y}_{ij})^2$	$MSLF = \frac{SSLF}{c-2}$	$F^* = \frac{MSLF}{MSPE}$
Total	n-1	$SSTD = \sum_{i=1}^{c}\sum_{j=1}^{ni}(y_{ij} - \bar{y}_{ij})^2$	-	-

RESULTS AND DISCUSSION

The design matrix showing the real value of three input variables namely; current (Amp), voltage (volts) and gas flow rate (L/min) and the response (fluidity) is presented in Figure 5

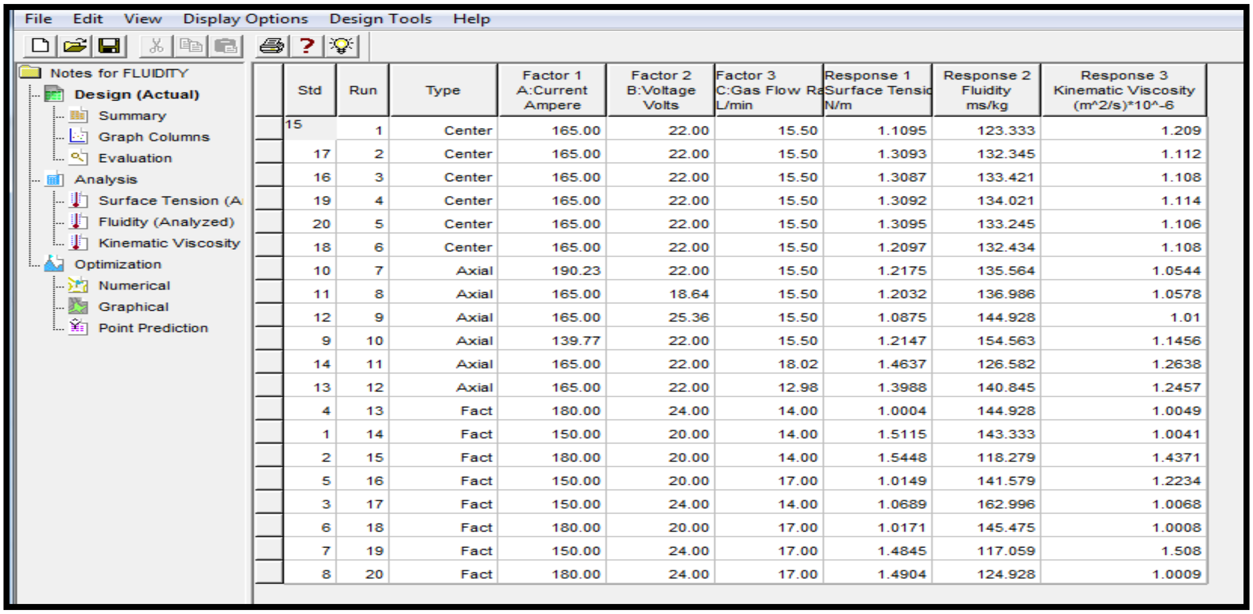

Std	Run	Type	Factor 1 A:Current Ampere	Factor 2 B:Voltage Volts	Factor 3 C:Gas Flow Ra L/min	Response 1 Surface Tensio N/m	Response 2 Fluidity ms/kg	Response 3 Kinematic Viscosity (m^2/s)*10^-6
15	1	Center	165.00	22.00	15.50	1.1095	123.333	1.209
17	2	Center	165.00	22.00	15.50	1.3093	132.345	1.112
16	3	Center	165.00	22.00	15.50	1.3087	133.421	1.108
19	4	Center	165.00	22.00	15.50	1.3092	134.021	1.114
20	5	Center	165.00	22.00	15.50	1.3095	133.245	1.106
18	6	Center	165.00	22.00	15.50	1.2097	132.434	1.108
10	7	Axial	190.23	22.00	15.50	1.2175	135.564	1.0544
11	8	Axial	165.00	18.64	15.50	1.2032	136.986	1.0578
12	9	Axial	165.00	25.36	15.50	1.0875	144.928	1.01
9	10	Axial	139.77	22.00	15.50	1.2147	154.563	1.1456
14	11	Axial	165.00	22.00	18.02	1.4637	126.582	1.2638
13	12	Axial	165.00	22.00	12.98	1.3988	140.845	1.2457
4	13	Fact	180.00	24.00	14.00	1.0004	144.928	1.0049
1	14	Fact	150.00	20.00	14.00	1.5115	143.333	1.0041
2	15	Fact	180.00	20.00	14.00	1.5448	118.279	1.4371
5	16	Fact	150.00	20.00	17.00	1.0149	141.579	1.2234
3	17	Fact	150.00	24.00	14.00	1.0689	162.996	1.0068
6	18	Fact	180.00	20.00	17.00	1.0171	145.475	1.0008
7	19	Fact	150.00	24.00	17.00	1.4845	117.059	1.508
8	20	Fact	180.00	24.00	17.00	1.4904	124.928	1.0009

Figure 5: Design matrix showing the real values and the experimental values

The model summary which shows the factors and their lowest and highest values including the mean and standard deviation is presented as shown in figure6; Result of figure 6 revealed that the model is of the quadratic type which requires the polynomial analysis order as depicted by a typical response surface design. For fluidity, the minimum value was observed to be 117.059ms/kg, with a maximum value of 162.996ms/kg, mean value of 136.842 and standard deviation of 11.222.

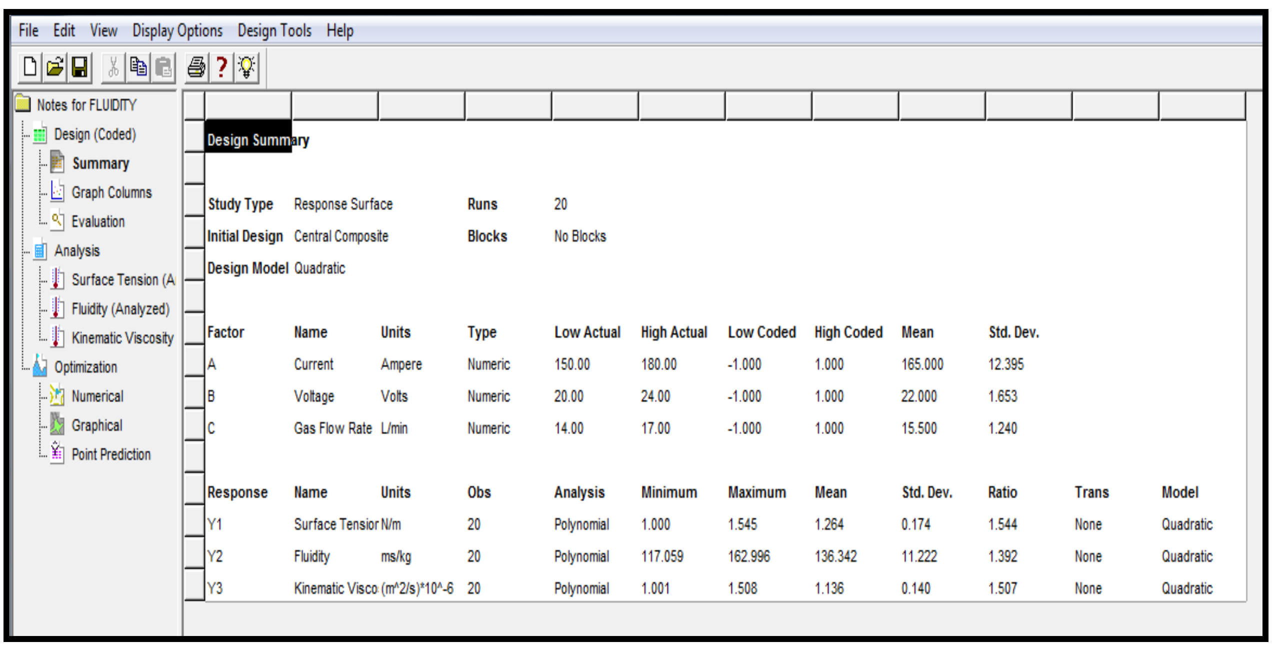

Design Summary

Study Type	Response Surface	Runs	20
Initial Design	Central Composite	Blocks	No Blocks
Design Model	Quadratic		

Factor	Name	Units	Type	Low Actual	High Actual	Low Coded	High Coded	Mean	Std. Dev.
A	Current	Ampere	Numeric	150.00	180.00	-1.000	1.000	165.000	12.395
B	Voltage	Volts	Numeric	20.00	24.00	-1.000	1.000	22.000	1.653
C	Gas Flow Rate	L/min	Numeric	14.00	17.00	-1.000	1.000	15.500	1.240

Response	Name	Units	Obs	Analysis	Minimum	Maximum	Mean	Std. Dev.	Ratio	Trans	Model
Y1	Surface Tensior	N/m	20	Polynomial	1.000	1.545	1.264	0.174	1.544	None	Quadratic
Y2	Fluidity	ms/kg	20	Polynomial	117.059	162.996	136.342	11.222	1.392	None	Quadratic
Y3	Kinematic Visco	(m^2/s)*10^-6	20	Polynomial	1.001	1.508	1.136	0.140	1.507	None	Quadratic

Figure 6: RSM design summary

To validate the suitability of the quadratic model in analyzing the experimental data, the sequential model sum of squares were calculated for Fluidity as presented in figure 7

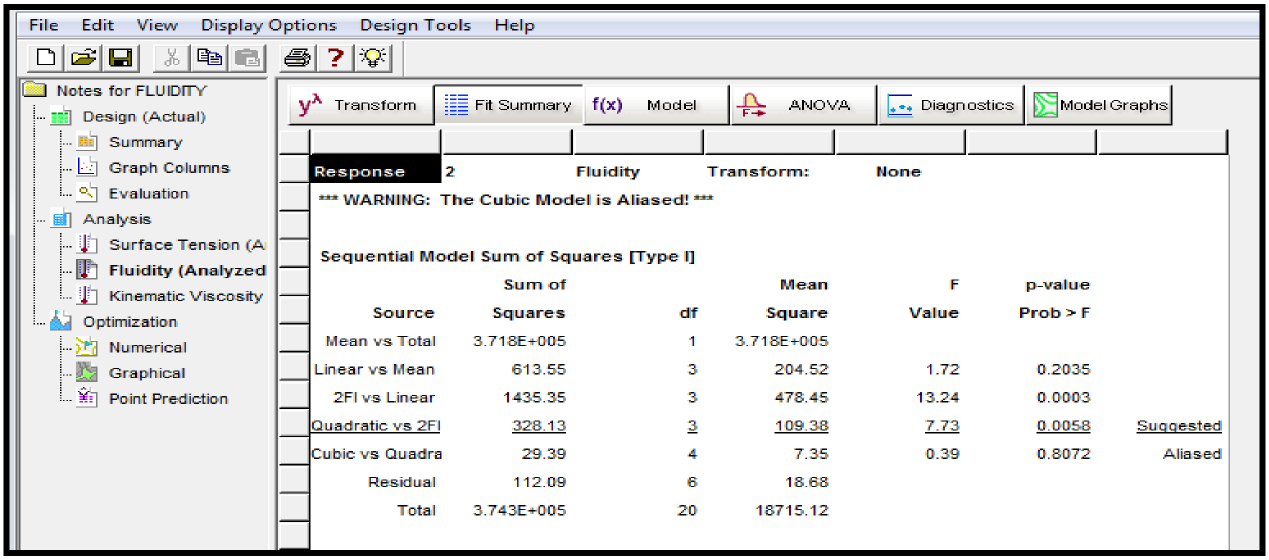

Response 2 Fluidity Transform: None

*** WARNING: The Cubic Model is Aliased! ***

Sequential Model Sum of Squares [Type I]

Source	Sum of Squares	df	Mean Square	F Value	p-value Prob > F	
Mean vs Total	3.718E+005	1	3.718E+005			
Linear vs Mean	613.55	3	204.52	1.72	0.2035	
2FI vs Linear	1435.35	3	478.45	13.24	0.0003	
Quadratic vs 2FI	328.13	3	109.38	7.73	0.0058	Suggested
Cubic vs Quadra	29.39	4	7.35	0.39	0.8072	Aliased
Residual	112.09	6	18.68			
Total	3.743E+005	20	18715.12			

Figure 7: Sequential model sum of square for Fluidity

The sequential model sum of squares table shows the accumulating improvement in the model fit as terms are added. Based on the calculated sequential model sum of square, the highest order polynomial where the additional terms are significant and the model is not aliased was selected as the best fit. From the results of figure 7 it was observed that the cubic polynomial was aliased hence cannot be employed to fit the final model. In addition, the quadratic and 2FI model were suggesed as the best fit thus justifying the use of quadratic polynomial in this analysis

To test how well the quadratic model can explain the underlying variation associated with the experimental data, the lack of fit test was estimated for fluidity. Model with significant lack of fit cannot be employed for prediction. Results of the computed lack of fit is presented in Figure 8

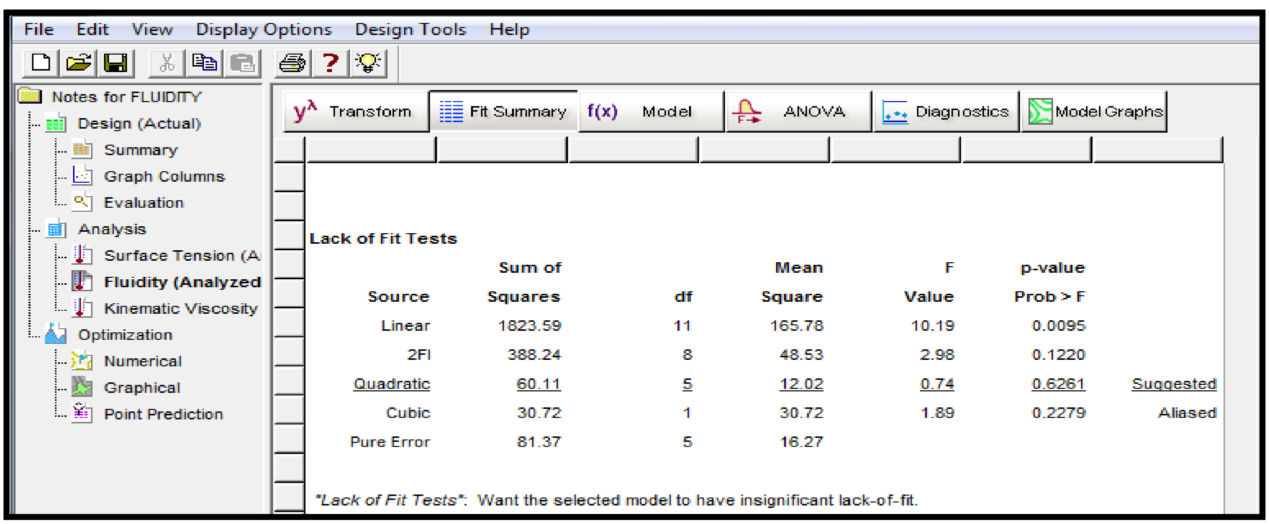

Lack of Fit Tests

Source	Sum of Squares	df	Mean Square	F Value	p-value Prob > F	
Linear	1823.59	11	165.78	10.19	0.0095	
2FI	388.24	8	48.53	2.98	0.1220	
Quadratic	60.11	5	12.02	0.74	0.6261	Suggested
Cubic	30.72	1	30.72	1.89	0.2279	Aliased
Pure Error	81.37	5	16.27			

"Lack of Fit Tests": Want the selected model to have insignificant lack-of-fit.

Figure 8: Lack of fit test for Fluidity

From the results of figure8, it was again observed that the quadratic polynomial had a non-significant lack of fit and was suggest for model analysis while the cubic polynomial had a significant lack of fit hence aliased to model analysis.

The model summary statistics computed for fluidity is presented in figure 9

Model Summary Statistics

Source	Std. Dev.	R-Squared	Adjusted R-Squared	Predicted R-Squared	PRESS	
Linear	10.91	0.2436	0.1018	-0.3443	3385.56	
2FI	6.01	0.8135	0.7275	0.6750	818.58	
Quadratic	3.76	0.9438	0.8933	0.7721	573.99	Suggested
Cubic	4.32	0.9555	0.8591	-1.7354	6889.12	Aliased

"Model Summary Statistics": Focus on the model maximizing the "Adjusted R-Squared" and the "Predicted R-Squared".

Figure 9: Model summary statistics for Fluidity

The model summary statistics of models fit shows the standard deviation (Root MSE), the r-squared and adjusted r-squared, predicted r-squared and the PRESS statistic for each complete model. Low standard deviation, R-Squared near unity and relatively low PRESS are the optimum criteria for defining the best model source. Based on the results of figure 9 the quadratic polynomial model was suggested while the cubic polynomial model was aliased hence, the quadratic polynomial model was selected for this analysis.

Analysis of the model standard error was employed to assess the suitability of response surface methodology using the quadratic model to maximize the fluidity. The computed standard errors for the selected responses is presented in figure 10

Term	StdErr**	VIF	Ri-Squared	Power at 5 % alpha level for effect of 0.5 Std. Dev.	1 Std. Dev.	2 Std. Dev.
A	0.27	1.00	0.0000	13.3 %	38.6 %	91.4 %
B	0.27	1.00	0.0000	13.3 %	38.6 %	91.4 %
C	0.27	1.00	0.0000	13.3 %	38.6 %	91.4 %
AB	0.35	1.00	0.0000	9.8 %	24.9 %	72.2 %
AC	0.35	1.00	0.0000	9.8 %	24.9 %	72.2 %
BC	0.35	1.00	0.0000	9.8 %	24.9 %	72.2 %
A^2	0.26	1.02	0.0179	40.4 %	92.7 %	99.9 %
B^2	0.26	1.02	0.0179	40.4 %	92.7 %	99.9 %
C^2	0.26	1.02	0.0179	40.4 %	92.7 %	99.9 %

**Basis Std. Dev. = 1.0

Figure 10: Result of computed standard errors

From the results of figure 10, it was observed that the model possess a low standard error ranging from 0.27 for the individual terms, 0.35 for the combine effects and 0.26 for the quadratic terms. Standard errors should be similar within type of coefficient; smaller is better. The error values were also observed to be less than the model basic standard deviation of 1.0 which suggests that response surface methodology was ideal for the optimization process. Variance inflation factor (VIF) of approximately 1.0 as observed in Table 11 was good since ideal VIF is 1.0. VIF's above 10 are cause for alarm, indicating coefficients are poorly estimated due to multicollinearity. In addition, the Ri-squared value was observed to be between 0.0000 to 0.0179 which is good. High Ri-squared (above 1.0) means that design terms are correlated with each other, possibly leading to poor models. The correlation matrix of regression coefficient is presented in figure 11

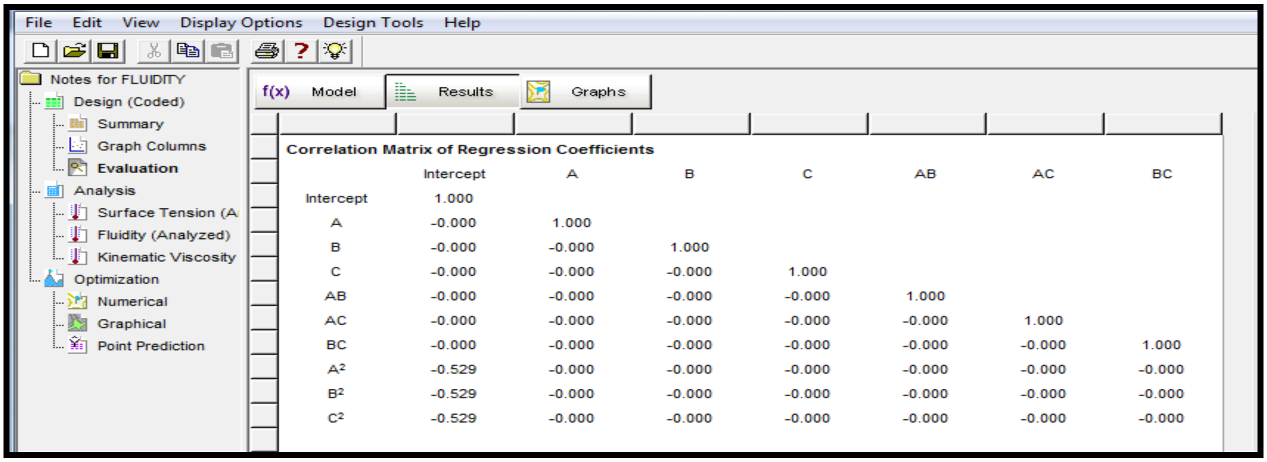

Correlation Matrix of Regression Coefficients

	Intercept	A	B	C	AB	AC	BC
Intercept	1.000						
A	-0.000	1.000					
B	-0.000	-0.000	1.000				
C	-0.000	-0.000	-0.000	1.000			
AB	-0.000	-0.000	-0.000	-0.000	1.000		
AC	-0.000	-0.000	-0.000	-0.000	-0.000	1.000	
BC	-0.000	-0.000	-0.000	-0.000	-0.000	-0.000	1.000
A^2	-0.529	-0.000	-0.000	-0.000	-0.000	-0.000	-0.000
B^2	-0.529	-0.000	-0.000	-0.000	-0.000	-0.000	-0.000
C^2	-0.529	-0.000	-0.000	-0.000	-0.000	-0.000	-0.000

Figure 11: Correlation matrix of regression coefficients

Lower values of the off diagonal matrix as observed in Table 11 indicates a well fitted model that is strong enough to navigate the design space and adequately optimize the selected response variables. From the results of figure 11, it was observed that the off diagonal matrix had coefficients that were approximately 0.00 which is an indication that the quadratic model was the ideal one for this analysis since off diagonal matrix greater than 0.00 is cause for alarm indicating a model having coefficients that are poorly correlated.

In assessing the strength of the quadratic model towards maximizing the fluidity, one way analysis of variance (ANOVA) was done and result is presented in figure 12

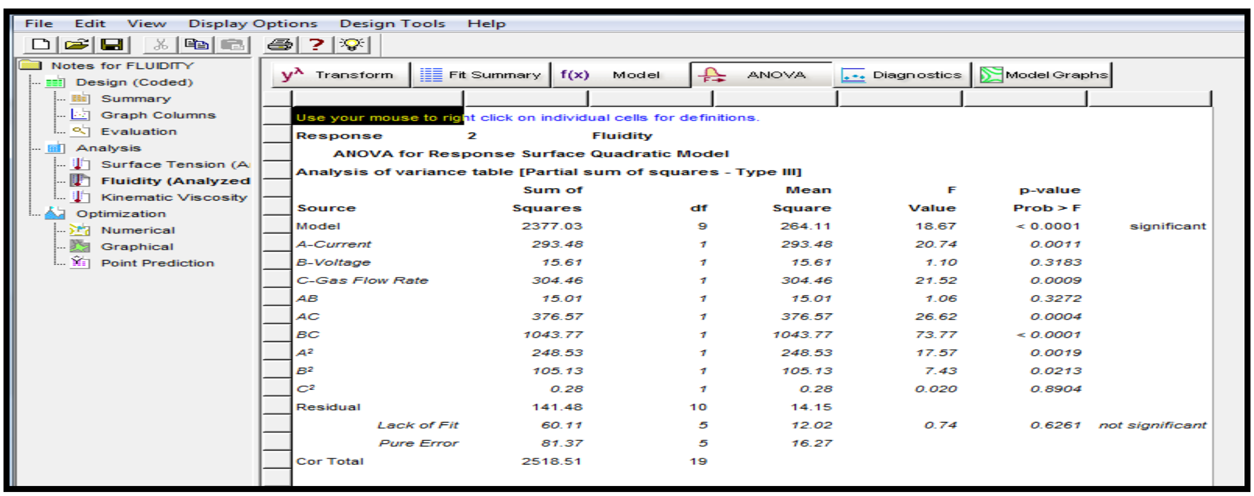

Use your mouse to right click on individual cells for definitions.

Response 2 Fluidity

ANOVA for Response Surface Quadratic Model

Analysis of variance table [Partial sum of squares - Type III]

Source	Sum of Squares	df	Mean Square	F Value	p-value Prob > F	
Model	2377.03	9	264.11	18.67	< 0.0001	significant
A-Current	293.48	1	293.48	20.74	0.0011	
B-Voltage	15.61	1	15.61	1.10	0.3183	
C-Gas Flow Rate	304.46	1	304.46	21.52	0.0009	
AB	15.01	1	15.01	1.06	0.3272	
AC	376.57	1	376.57	26.62	0.0004	
BC	1043.77	1	1043.77	73.77	< 0.0001	
A^2	248.53	1	248.53	17.57	0.0019	
B^2	105.13	1	105.13	7.43	0.0213	
C^2	0.28	1	0.28	0.020	0.8904	
Residual	141.48	10	14.15			
Lack of Fit	60.11	5	12.02	0.74	0.6261	not significant
Pure Error	81.37	5	16.27			
Cor Total	2518.51	19				

Figure 12: ANOVA table for validating the model significance towards maximizing the fluidity

Analysis of variance (ANOVA) was needed to check whether or not the model is significant and also to evaluate the significant contributions of each individual variable, the combined and quadratic effects towards each response.

From the result of figure 12, the Model F-value of 18.67 implies the model is significant. There is only a 0.01% chance that a "Model F-Value" this large could occur due to noise. Values of "Prob > F" less than 0.0500 indicate model terms are significant. In this case A, C, AC, BC, A2, B2 are significant model terms. Values greater than 0.1000 indicate the model terms are not significant. The "Lack of Fit F-value" of 0.74 implies the Lack of Fit is not significant relative to the pure error. There is a 62.61% chance that a "Lack of Fit F-value" this large could occur due to noise. Non-significant lack of fit is good as it indicates a model that is significant.

To validate the adequacy of the quadratic model based on its ability to maximize the fluidity and, the goodness of fit statistics presented in figure 13 was employed;

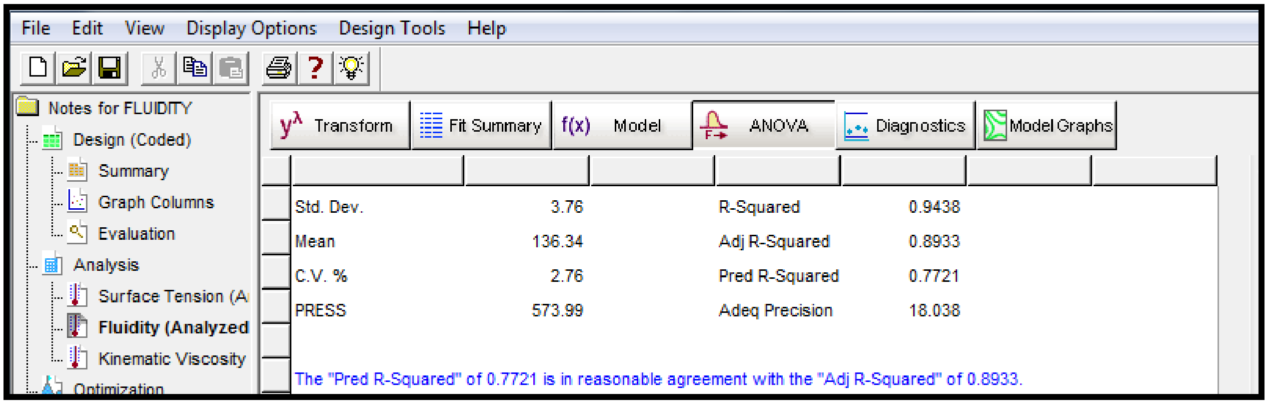

Std. Dev.	3.76	R-Squared	0.9438
Mean	136.34	Adj R-Squared	0.8933
C.V. %	2.76	Pred R-Squared	0.7721
PRESS	573.99	Adeq Precision	18.038

The "Pred R-Squared" of 0.7721 is in reasonable agreement with the "Adj R-Squared" of 0.8933.

Figure 4.19: GOF statistics for validating model significance towards maximizing fluidity

From the result of figure 13, it was observed that the "Predicted R-Squared" value of 0.7721 is in reasonable agreement with the "Adj R-Squared" value of 0.8933. Adequate precision measures the signal to noise ratio. A ratio greater than 4 is desirable. The computed ratio of 18.038as observed in figure 13 indicates an adequate signal. This model can be used to navigate the design space and maximize the fluidity

To obtain the optimal solution, we first consider the coefficient statistics and the corresponding standard errors. The computed standard error measures the difference between the experimental terms and the corresponding predicted terms. Coefficient statistics for fluidity is presented in figure 14

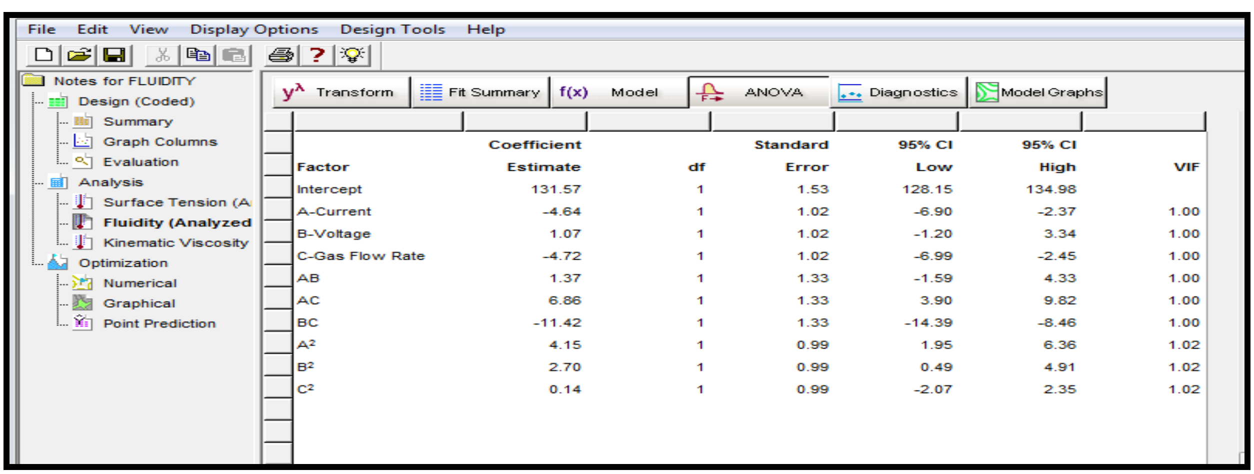

Factor	Coefficient Estimate	df	Standard Error	95% CI Low	95% CI High	VIF
Intercept	131.57	1	1.53	128.15	134.98	
A-Current	-4.64	1	1.02	-6.90	-2.37	1.00
B-Voltage	1.07	1	1.02	-1.20	3.34	1.00
C-Gas Flow Rate	-4.72	1	1.02	-6.99	-2.45	1.00
AB	1.37	1	1.33	-1.59	4.33	1.00
AC	6.86	1	1.33	3.90	9.82	1.00
BC	-11.42	1	1.33	-14.39	-8.46	1.00
A^2	4.15	1	0.99	1.95	6.36	1.02
B^2	2.70	1	0.99	0.49	4.91	1.02
C^2	0.14	1	0.99	-2.07	2.35	1.02

Figure 14: Coefficient estimates statistics towards maximizing fluidity

The optimal equation which shows the individual effects and combines interactions of the selected input variables (current, voltage and gas flow rate) against (fluidity) is presented based on the coded variables in figure 15.

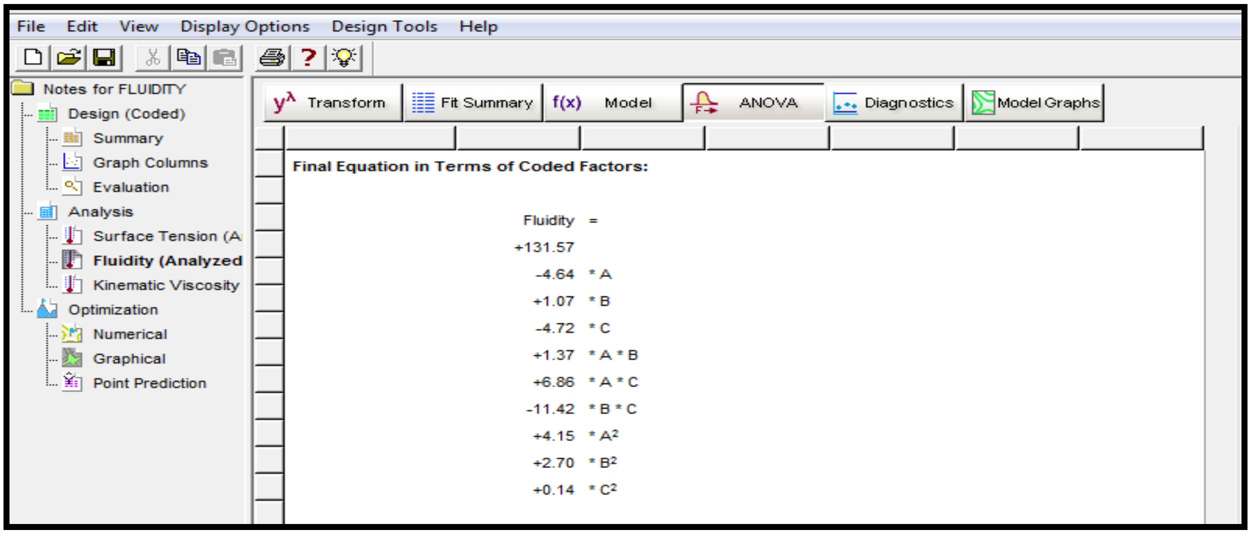

Figure 15: Optimal equation in terms of coded factors for maximizing fluidity

The optimal equation which shows the individual effects and combine interactions of the selected input variables (current, voltage and gas flow rate) against (fluidity is presented in actual factors in figure 16

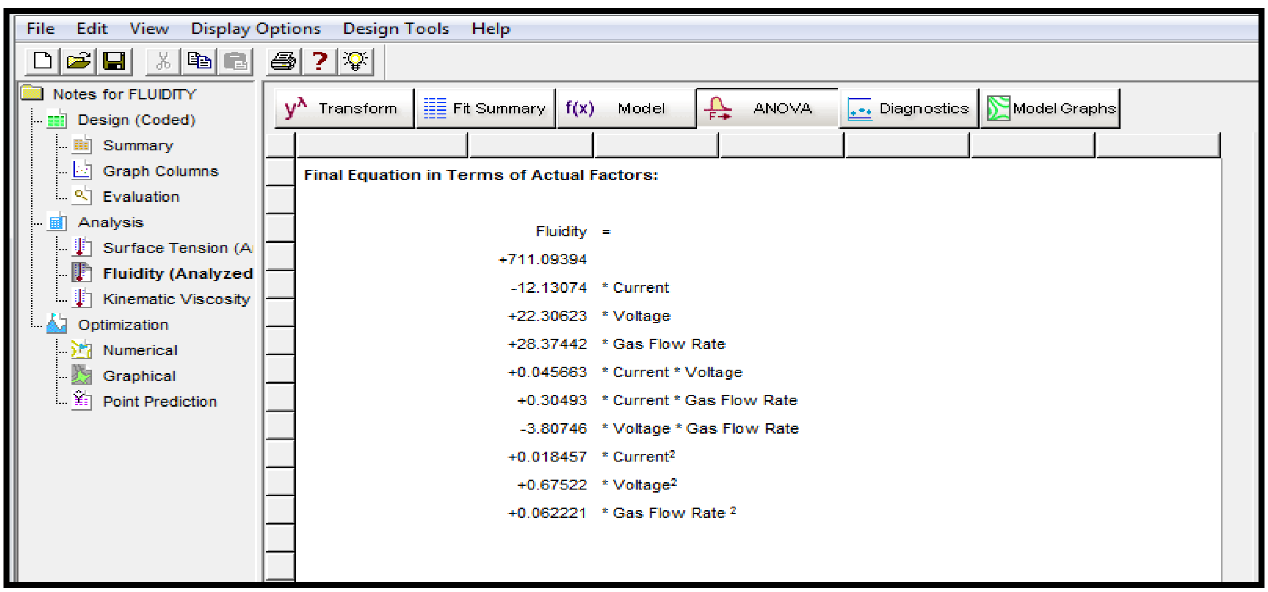

Figure 16: Optimal equation in terms of actual factors for maximizing fluidity

The diagnostics case statistics which shows the observed values of each response variable (fluidity) against the predicted values is presented in figure 17 the diagnostic case statistics actually give insight into the model strength and the adequacy of the optimal second order polynomial equation.

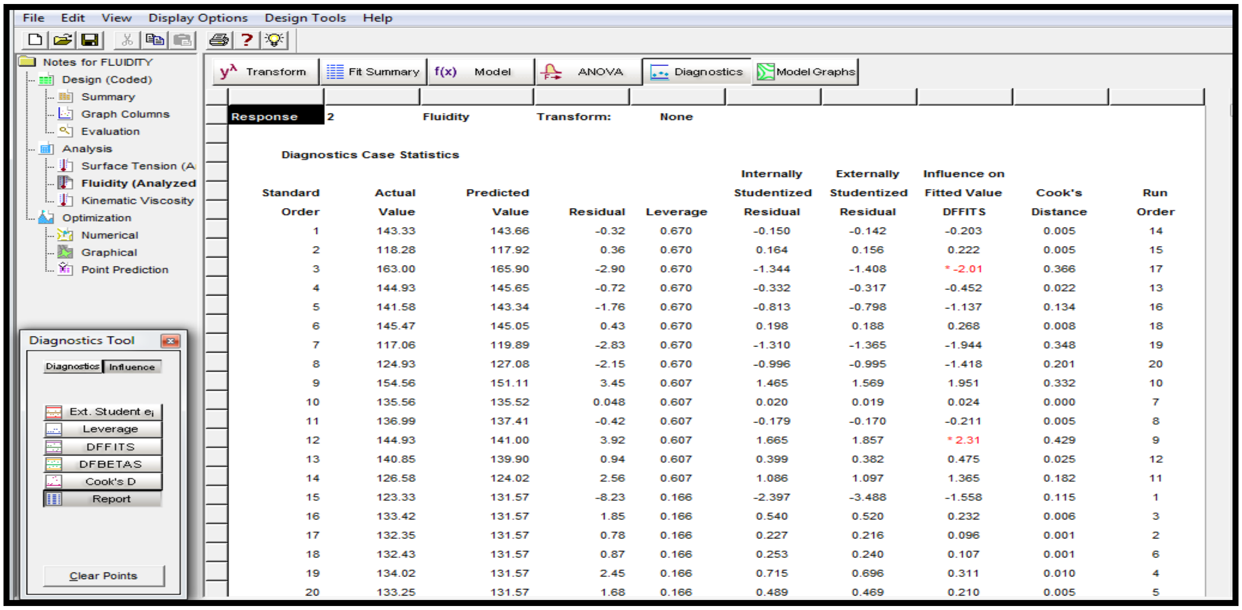

Response 2 Fluidity Transform: None

Diagnostics Case Statistics

Standard Order	Actual Value	Predicted Value	Residual	Leverage	Internally Studentized Residual	Externally Studentized Residual	Influence on Fitted Value DFFITS	Cook's Distance	Run Order
1	143.33	143.66	-0.32	0.670	-0.150	-0.142	-0.203	0.005	14
2	118.28	117.92	0.36	0.670	0.164	0.156	0.222	0.005	15
3	163.00	165.90	-2.90	0.670	-1.344	-1.408	* -2.01	0.366	17
4	144.93	145.65	-0.72	0.670	-0.332	-0.317	-0.452	0.022	13
5	141.58	143.34	-1.76	0.670	-0.813	-0.798	-1.137	0.134	16
6	145.47	145.05	0.43	0.670	0.198	0.188	0.268	0.008	18
7	117.06	119.89	-2.83	0.670	-1.310	-1.365	-1.944	0.348	19
8	124.93	127.08	-2.15	0.670	-0.996	-0.995	-1.418	0.201	20
9	154.56	151.11	3.45	0.607	1.465	1.569	1.951	0.332	10
10	135.56	135.52	0.048	0.607	0.020	0.019	0.024	0.000	7
11	136.99	137.41	-0.42	0.607	-0.179	-0.170	-0.211	0.005	8
12	144.93	141.00	3.92	0.607	1.665	1.857	* 2.31	0.429	9
13	140.85	139.90	0.94	0.607	0.399	0.382	0.475	0.025	12
14	126.58	124.02	2.56	0.607	1.086	1.097	1.365	0.182	11
15	123.33	131.57	-8.23	0.166	-2.397	-3.488	-1.558	0.115	1
16	133.42	131.57	1.85	0.166	0.540	0.520	0.232	0.006	3
17	132.35	131.57	0.78	0.166	0.227	0.216	0.096	0.001	2
18	132.43	131.57	0.87	0.166	0.253	0.240	0.107	0.001	6
19	134.02	131.57	2.45	0.166	0.715	0.696	0.311	0.010	4
20	133.25	131.57	1.68	0.166	0.489	0.469	0.210	0.005	5

Figure 17: Diagnostics case statistics report of observed and predicted fluidity

To assess the accuracy of prediction and established the suitability of response surface methodology using the quadratic model, a reliability plot of the observed and predicted values of fluidity was obtained as presented in Figures 18

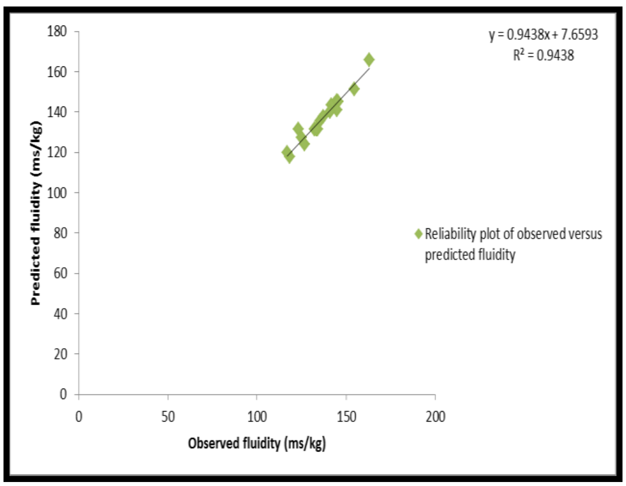

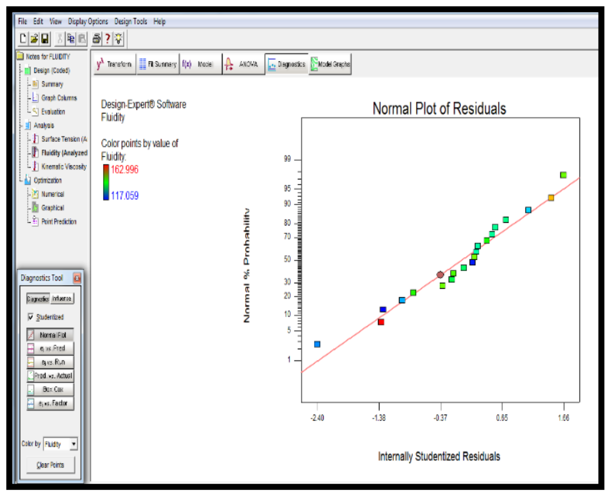

Figure 18: Reliability plot of observed versus predicted Fluidity Figure 19: Normal probability plot of student zed residuals for Fluidity

To accept any model, its satisfactoriness must first be checked by an appropriate statistical analysis output. To diagnose the statistical properties of the fluidity model, the normal probability plot of residual presented in Figure 19

The normal probability plot of student zed residuals was employed to assess the normality of the calculated residuals. Results of Figures 19revealed that the computed residuals are approximately normally distributed an indication that the model developed is satisfactory and the data employed are devoid of possible outliers.

To determine the presence of a possible outlier, the cook's distance plot was generated for the fluidity. The cook's distance is a measure of how much the regression would change if the outlier is omitted from the analysis. A point that has a very high distance value relative to the other points may be an outlier and should be investigated. The generated cook's distance is presented in Figures 20

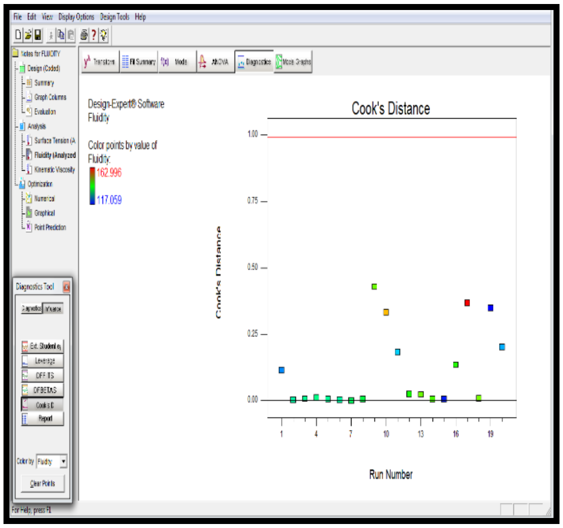

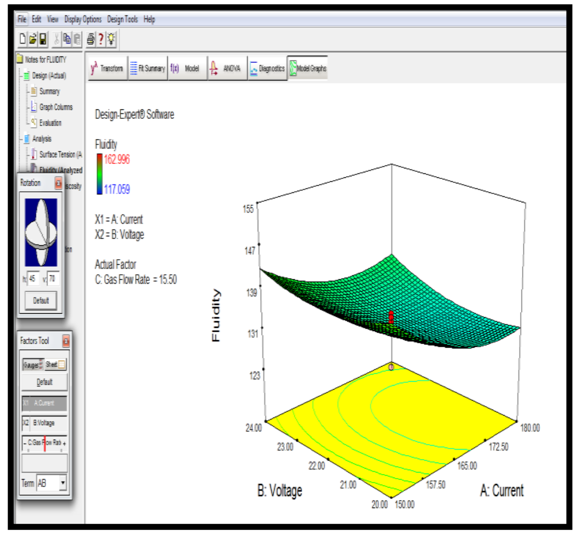

Figure 20: Generated cook's distance for Fluidity Figure 21: Effect of current and voltage on fluidity

To study the effects of combine input variables on fluidity 3D surface plots is presented in Figure 21 The 3D surface plot as observed in Figure 22 shows the relationship between the input variables (current, voltage and gas flow rate) and the response variable (fluidity). It is a 3 dimensional surface plot which was employed to give a clearer concept of the response surface. Although not as useful as the contour plot for establishing responses values and coordinates, this view may provide a clearer view of the surface. As the colour of the curved surface gets darker, the fluidity increases. The presence of a coloured hole at the middle of the upper surface gave a clue that more points lightly shaded for easier identification fell below the surface.

Finally, numerical optimization was performed to ascertain the desirability of the overall model. In the numerical optimization phase, we ask design expert to determine the optimum current (Amp), voltage (volts) and gas flow rate (L/min) that will maximize fluidity The interphase of the numerical optimization showing the objective function is presented in Figure 23

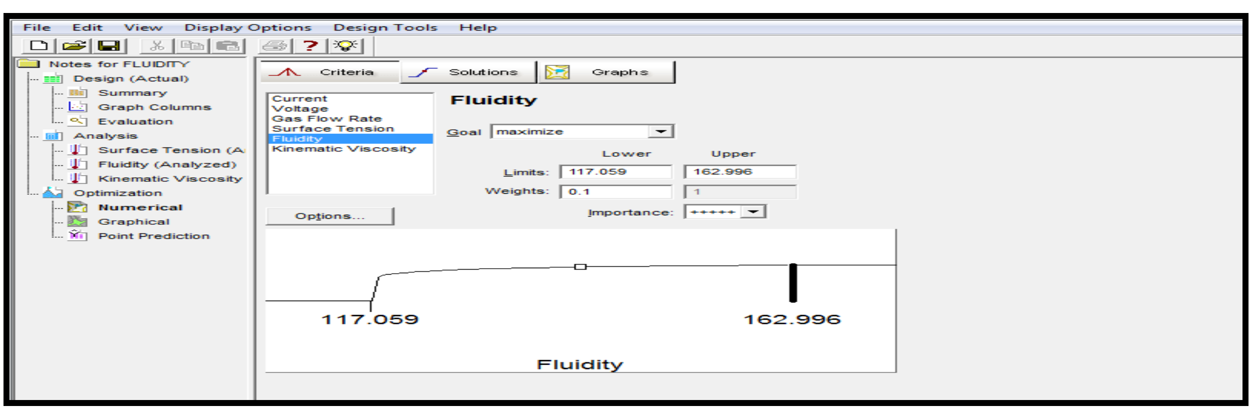

Figure 23: Interphase of numerical optimization model for maximizing the fluidity

The numerical optimization generated about sixteen (16) optimal solutions which are presented in figure 24

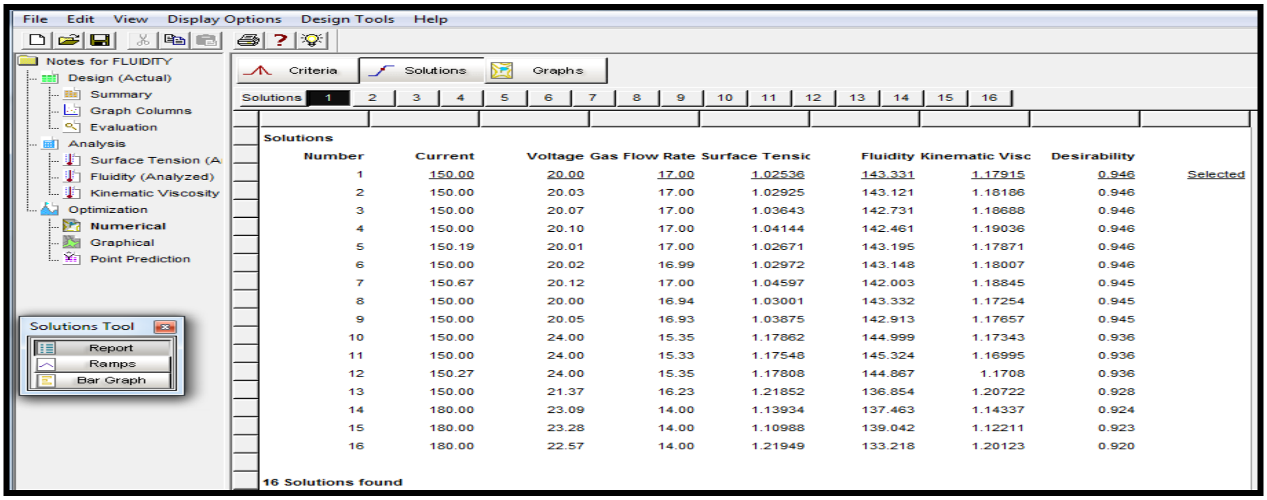

Solutions

Number	Current	Voltage	Gas Flow Rate	Surface Tensic	Fluidity	Kinematic Visc	Desirability	
1	150.00	20.00	17.00	1.02536	143.331	1.17915	0.946	Selected
2	150.00	20.03	17.00	1.02925	143.121	1.18186	0.946	
3	150.00	20.07	17.00	1.03643	142.731	1.18688	0.946	
4	150.00	20.10	17.00	1.04144	142.461	1.19036	0.946	
5	150.19	20.01	17.00	1.02671	143.195	1.17871	0.946	
6	150.00	20.02	16.99	1.02972	143.148	1.18007	0.946	
7	150.67	20.12	17.00	1.04597	142.003	1.18845	0.945	
8	150.00	20.00	16.94	1.03001	143.332	1.17254	0.945	
9	150.00	20.05	16.93	1.03875	142.913	1.17657	0.945	
10	150.00	24.00	15.35	1.17862	144.999	1.17343	0.936	
11	150.00	24.00	15.33	1.17548	145.324	1.16995	0.936	
12	150.27	24.00	15.35	1.17808	144.867	1.1708	0.936	
13	150.00	21.37	16.23	1.21852	136.854	1.20722	0.928	
14	180.00	23.09	14.00	1.13934	137.463	1.14337	0.924	
15	180.00	23.28	14.00	1.10988	139.042	1.12211	0.923	
16	180.00	22.57	14.00	1.21949	133.218	1.20123	0.920	

16 Solutions found

Figure 24: Optimal solutions of numerical optimization model

From the results of figure 24, it was observed that a current of 150amp, voltage of 20volts and gas flow rate of 17.00L/min will produce a weld material with, Fluidity of 143.331ms/kg. This solution was selected by design expert as the optimal solution with a desirability value of 94.60%.

The desirability bar graph which shows the accuracy with which the model is able to predict the values of the selected input variables and the corresponding responses is presented in Figure 25.

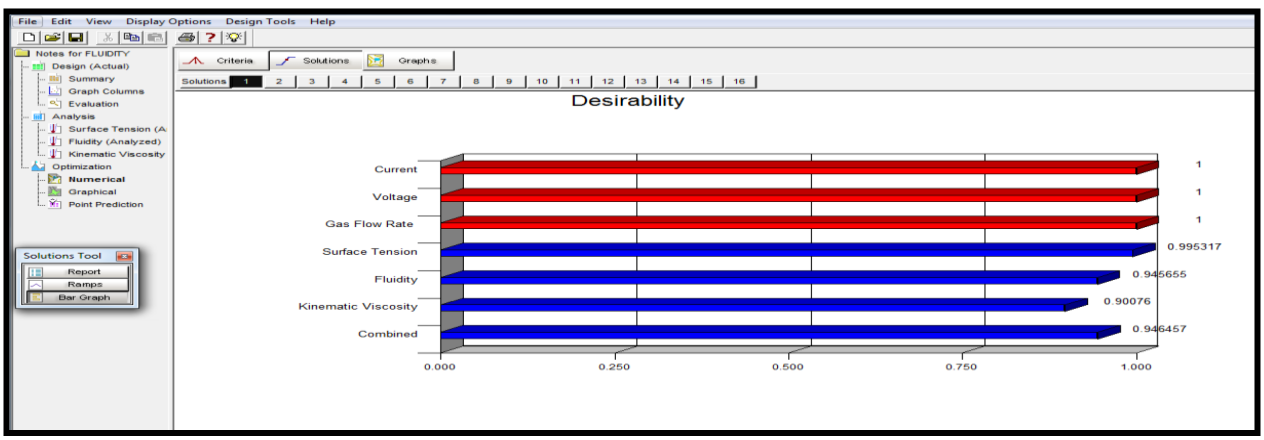

Figure 25: Prediction accuracy of numerical optimzation

It can be deduce from the result of Figure 25 that the model developed based on response surface methodology and optimized using numerical optimization method, predicted Fluidity with an accuracy level of 94.57%

The contour plots showing fluidity variable against the optimized value of the input variable is presented in Figure 26

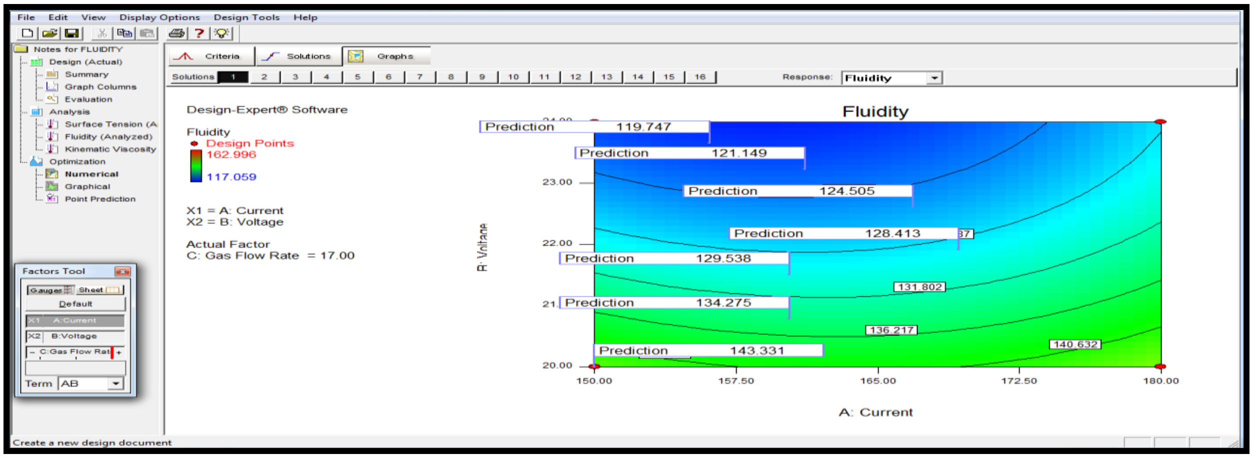

Figure 26: Predicting fluidity using contour plot

A plot of desirability against the input variables is presented in figure 27

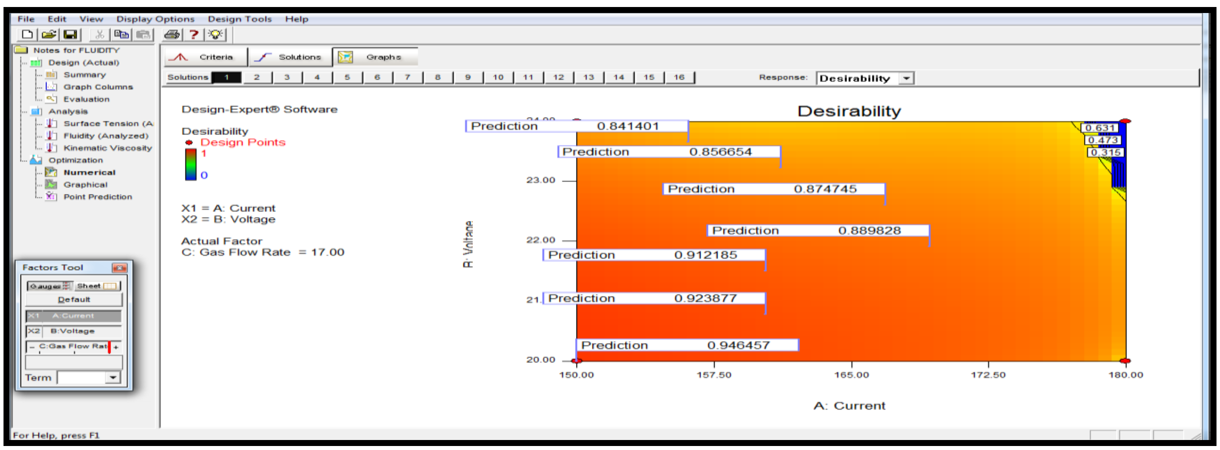

Figure 27: Predicting desirability using contour plot

As presented in Figures 27, the contour plot can be employed to predict the optimum values of the input variables based on the flagged response variables.

Conclusion

In this study, the response surface methodology was used to optimize the molten, metal properties such as fluidity of gas tungsten arc mild steel welds. A model was developed using the Response surface methodology (RSM), the Result revealed that the model is of the quadratic type which requires the polynomial analysis order as depicted by a typical response surface design.

In assessing the strength of the quadratic model towards optimizing molten metal fluidity, one way analysis of variance (ANOVA) was done for each response variable. To validate the adequacy of the model based on its ability to predict its target response, the goodness of fit statistics was employed. Coefficient of determination R2 values of 0.9438 for metal fluidity model.

Adeq Precision measures the signal to noise ratio. A ratio greater than 4 is desirable. Adequate precision values of 18.038 which indicates adequate signal. The diagnostic case statistics actually give insight into the model strength and the adequacy of the optimal second order polynomial equation. To assess the accuracy of prediction and established the suitability of response surface methodology using the quadratic model, a reliability plot of the observed and predicted values of each response were obtained.

From the results, it was observed that a current of 150.00 Amp, voltage of 20 volt and a gas flow rate of 17 L/min will produce a welded material having fluidity 143.331 at a desirability of 0.946. Response surface methodology using numerical optimization was effective in predicting the fluidity. It was also relevant in determining the exact mathematical relationship between the input parameters (voltage, current and gas flow rate) and the response variables.

Reference

Di Sabatino, M.; Amberg, L. And Apelian, D. (2008) Progress on the Understanding of Fluidity of Aluminium Foundry Alloys. International Journal of Metal casting, Vol. 2, Issue 3, pp. 17-27.

Morando C, Fornaro O, Garbellini O and Palacio H (2015) "Fluidity on Metallic Eutectic Alloys" International Congress of Science and Technology of Metallurgy and Materials. Procedia Materials Science 8, pp. 959-967.

Davies, M.H. (1992) Numerical Modelling of Weld Pool Convection in Gas Metal Arc Welding. Doctor of Philosophy. Thesis. Department of Mechanical Engineering. The University of Adelaide, South Australia.

Nasim Bakir, Antoni Artinov, Andrey Gumenyuk, Marcel Bachmann and Michael Rethmeier, (2018). Numerical Simulation on the Origin of Solidification Cracking in Laser Welded Thick-Walled Structures. Metals 2018, 8, 406; doi:10.3390/met8060406

R.T.C. Choo, J. Szekely and R.C. Westh off: 'On the calculation of the free surface temperature of gas-tungsten-arc weld pools from first principles: part 1. modeling the welding arc', Metallurgical Transactions B, 1992, 23B, 357-369

S. Kou and Y.H. Wang: 'Weld pool convection and its effect', Welding Journal, 1986,65(3), 63-70.

S. Kou, C. Limmaneevichitr and P.S. Wei: 'Oscillatory Marangoni flow: a fundamental study by conduction-mode laser spot welding', Welding Journal, 2011, 90(12), 229-240

Chen,C.M. and Kovacevic, R. "Joining of Al 6061 alloy to AISI 1018 steel by combined effects of fusion and solid state welding", International Journal of Machine Tools & Manufacture ,44: 1205–1214, 2004

Bakhtiyarov, S.I. and Over felt, R.A... (1999). Measurement of Liquid Metal Viscosity by Rotational Technique, Acta Metallurgica Inc. 47, (17); pp. 4311 – 4319.

Ambroziak, (1999) "Friction Welding in a Liquid - A New Technology for Bonding Special Metals", Proc XXXV Polish Welding conference, Czestochowa, 160-169, 1999.